Electronic Supplementary Information (ESI)

Computational Studies on Functionalized Janus MXenes $MM'CT_2$, (M, M′=Zr, Ti, Hf, M ≠ M′; T = -O, -F, -OH): Photoelectronic Properties and Potential Photocatalytic Activities

Kuangwei Xiong,*[a] Ziqiang Cheng,[a] Jianpeng Liu,[a] Peng-Fei Liu,[b] Zhenfa Zi[c]

[a] Department of Physics, East China Jiaotong University, Nanchang 330013, P.R. China

[b] *Institute of High Energy Physics, Chinese Academy of Sciences, Beijing 100049, P.R. China*

[c] School of Physics and Materials Engineering, Hefei Normal University, Hefei 230601, P.R. China

* E-mail: xiongkw@ecjtu.edu.cn;

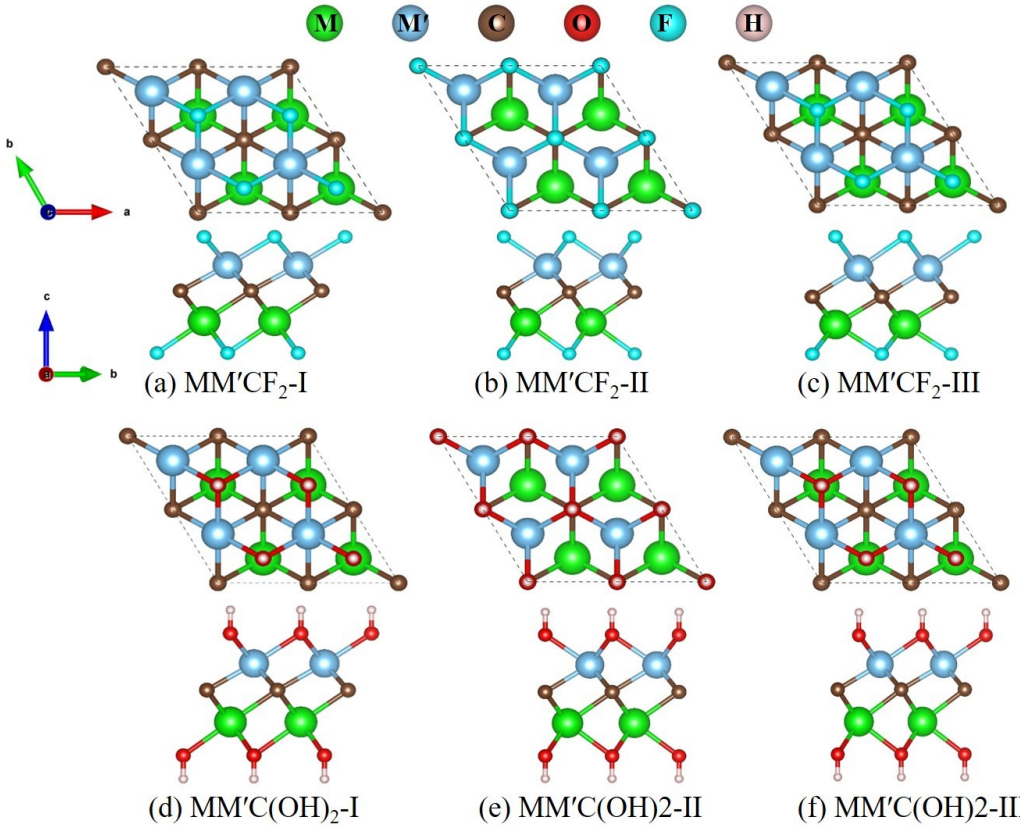

Fig. S1 Top view (top) and side view (bottom) of geometries of (a–c) $MM'CF_2$-I, II, III; (d–f) $MM'C(OH)_2$-I, II, III. M, M′ = Zr, Ti, Hf; M≠M′.

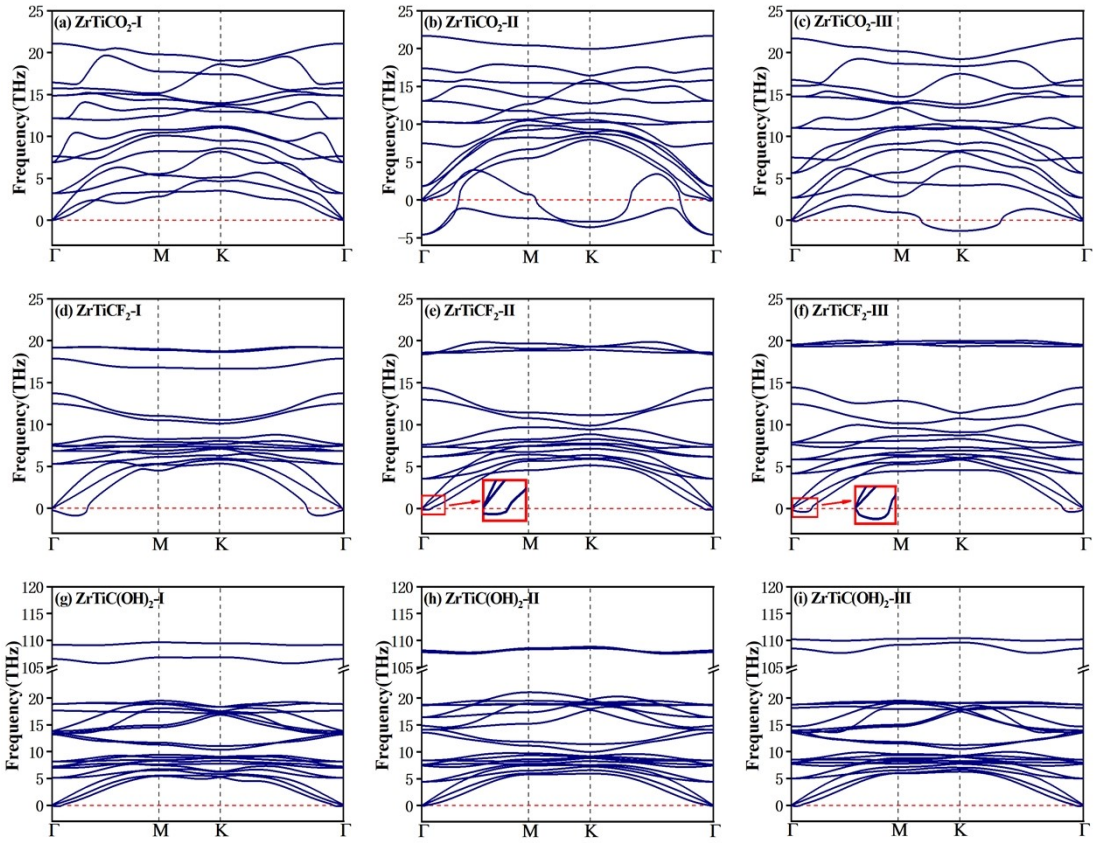

Fig. S2 Phonon dispersion of surface-functionalized ZrTiC MXenes with $ZrTiCT_2$-I, $ZrTiCT_2$-II, and $ZrTiCT_2$-III structures (T = -O, -F, and -OH). The insets in (e) and (f) display magnified images of the acoustic branches around the Γ-point.

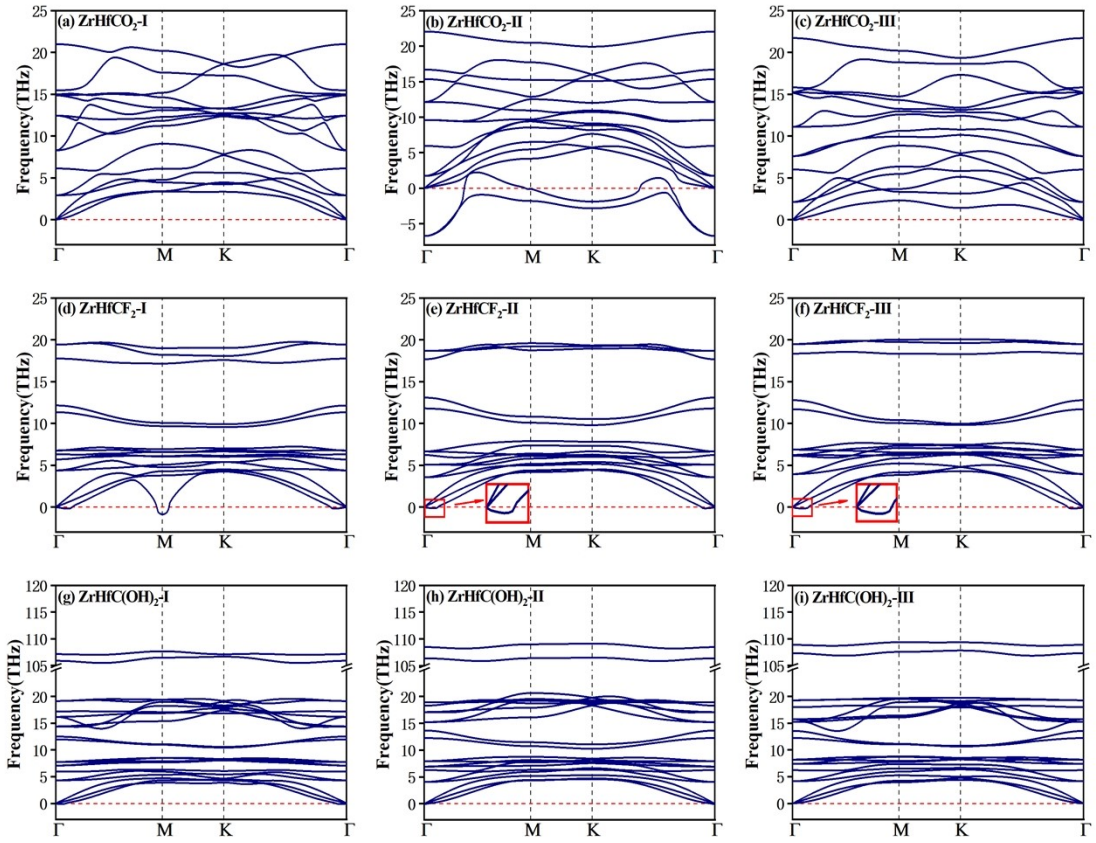

Fig. S3 Phonon dispersion of surface-functionalized ZrHfC MXenes with $ZrHfCT_2$-I, $ZrHfCT_2$-II, and $ZrHfCT_2$-III structures (T = -O, -F, and -OH). The insets in (e) and (f) display magnified images of the acoustic branches around the Γ-point.

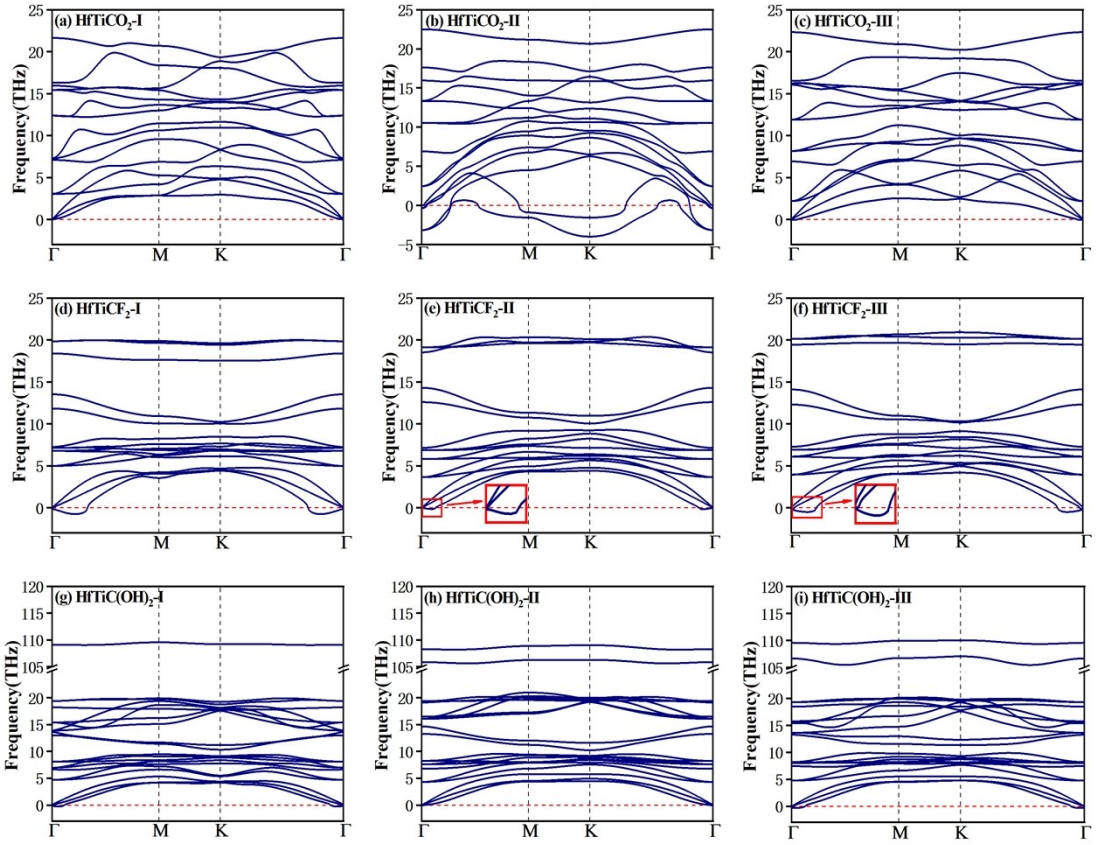

Fig. S4 Phonon dispersion of surface-functionalized HfTiC MXenes with $HfTiCT_2$-I, $HfTiCT_2$-II, and $HfTiCT_2$-III structures (T = -O, -F, and -OH). The insets in (e) and (f) display magnified images of the acoustic branches around the Γ-point.

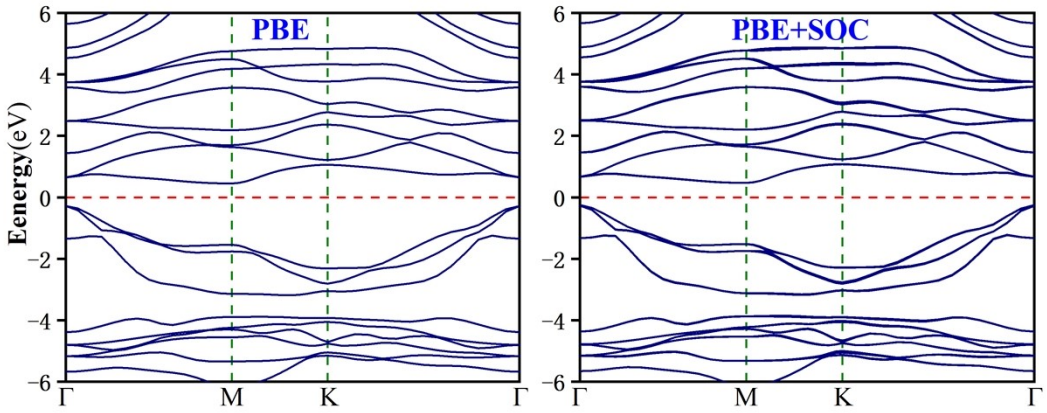

Fig. S5 Band structures of $ZrTiCO_2$-I with PBE and PBE+SOC methods. The red dashed lines mark the Fermi level at 0 eV.

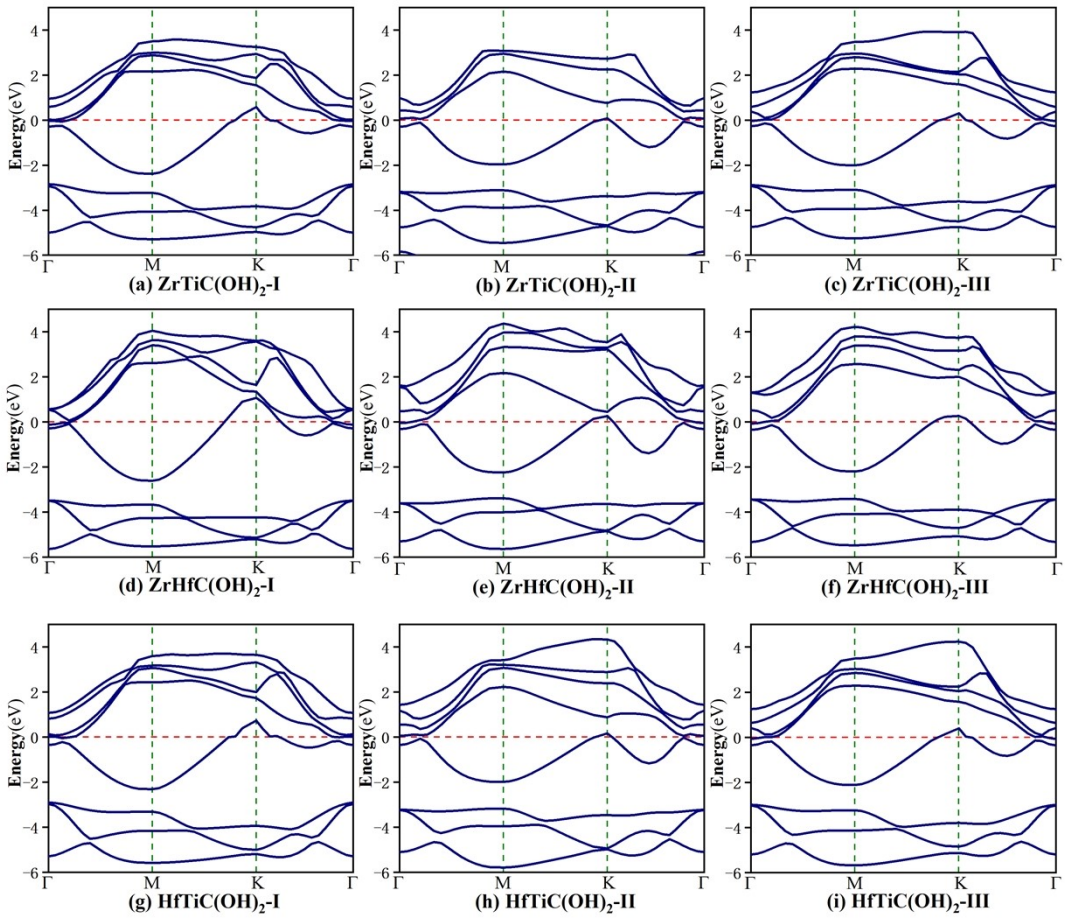

Fig. S6 Band structures of (a) $ZrTiC(OH)_2$-I, (b) $ZrTiC(OH)_2$-II, (c) $ZrTiC(OH)_2$-III, (d) $ZrHfC(OH)_2$-I, (e) $ZrHfC(OH)_2$-II, (f) $ZrHfC(OH)_2$-III, (g) $HfTiC(OH)_2$-I, (h) $HfTiC(OH)_2$-II, and (i) $HfTiC(OH)_2$-III. The red dashed lines mark the Fermi level at 0 eV.

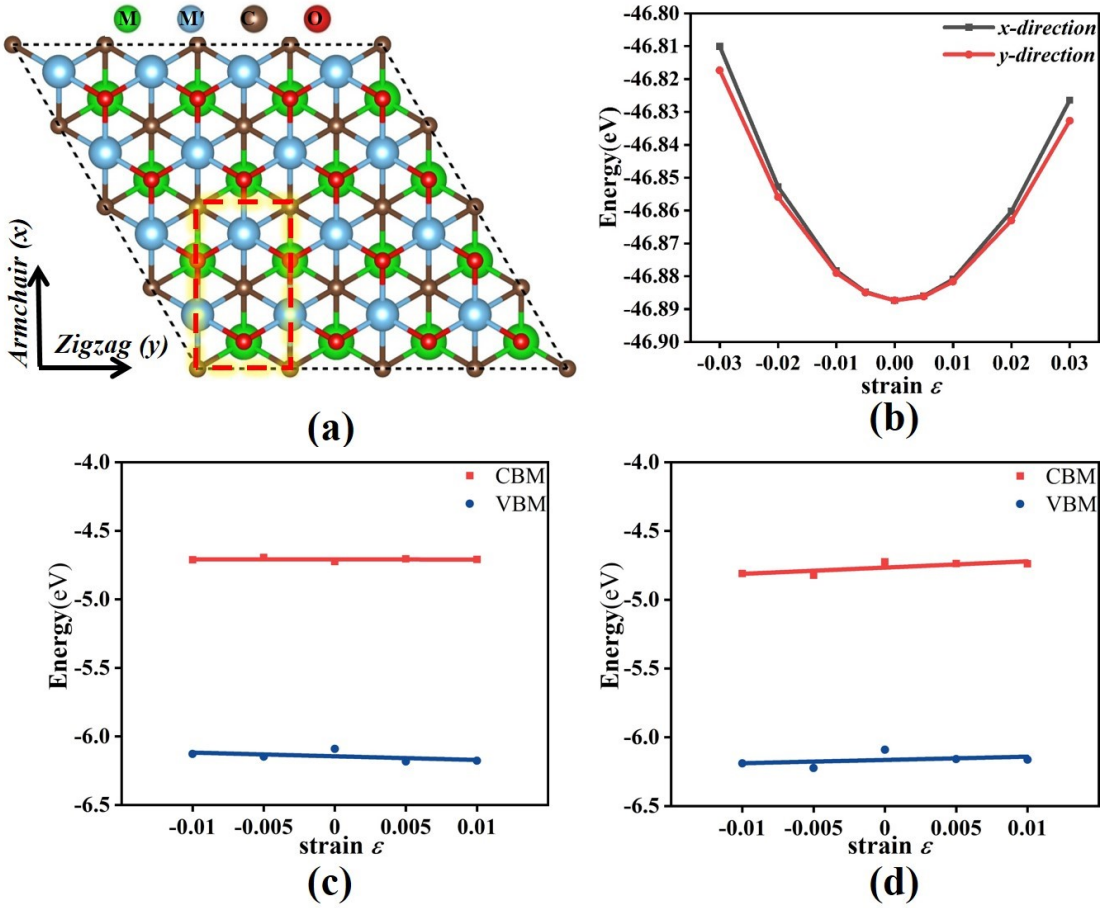

Fig. S7 (a) $ZrTiCO_2$-I Janus monolayer; the black and red dashed lines represent a 4×4 hexagonal supercell and the orthogonal primitive cell, respectively. (b) Relationship between total energy and uniaxial strain along the *x* and *y* directions. (c,d) Shift of band edge position with respect to the uniaxial strain along the (c) *x*- and, (d) *y*-direction.

Details of Carrier Mobility Calculations

As an example, we describe the calculations of the electron carrier mobility along the *x* direction of the $ZrTiCO_2$-I Janus monolayer. To obtain the elastic modulus *C* and deformation potential constant E_1, we calculated the total energy and band edge positions as a function of the uniaxial strain ε, as shown in Fig. S6(b,c). The calculated results are listed in Table S4.

To calculate the effective mass, we plotted the relationship between the energy *E(k)* and the wave vector *k* with 30 high-density *k*-points near the CBM, then employed a second-order polynomial function to fit the curve:

$$E(k) = Intercept + B_1 k + B_2 k^2$$

The second derivative of the fitting function is:

$$\left.\frac{\partial^2 E(k)}{\partial k^2}\right|_{k=M(0.5,0,0)} = 2B_2$$

According to the definition of carrier effective mass, the electron effective mass along the *x*-direction can be calculated as:

$$m^* = \hbar^2 / (\partial^2 E(k) / \partial k^2) = \hbar^2 / 2B_2$$

Table S1 Cohesive energies (E_{coh}, eV/atom) of functionalized Janus MXenes.

	$ZrTiCT_2$			$ZrHfCT_2$			$HfTiCT_2$		
	T=O	T=F	T=OH	T=O	T=F	T=OH	T=O	T=F	T=OH
Geometry I	7.59	6.88	5.99	8.14	7.25	6.28	7.78	6.99	6.09
Geometry II	7.20	6.79	5.95	7.71	7.19	6.25	7.38	6.90	6.05
Geometry III	7.42	6.82	6.00	7.96	7.26	6.29	7.60	6.94	6.08

Table S2 Band gaps (E_g, eV) of MM′CT_2 with differently functionalized geometries calculated at the HSE06 level. The M label denotes metallic properties of the corresponding MM′CT_2 material.

	$ZrTiCT_2$			$ZrHfCT_2$			$HfTiCT_2$		
	T=O	T=F	T=OH	T=O	T=F	T=OH	T=O	T=F	T=OH
MM′CT_2-I	1.37	none	M	1.71	none	M	1.43	none	M
MM′CT_2-II	none	none	M	none	none	M	none	none	M
MM′CT_2-III	none	none	M	1.77	none	M	1.94	none	M

Table S3 Vacuum level, CBM and VBM levels (eV) of $ZrTiCO_2$-I, $ZrHfCO_2$-I, $ZrHfCO_2$-III, $HfTiCO_2$-I, and $ZrHfCO_2$-III. E_{CBM} and E_{VBM} denote band edge positions, whose value are listed relative to the Fermi level, vacuum level and normal hydrogen electrode (E_{NHE} = -4.5 eV), respectively.

	E_{Vacuum}	E_{Fermi}	E_{CBM}			E_{VBM}		
			vs. Fermi	*vs.* vacuum	*vs.* NHE	*vs.* Fermi	*vs.* vacuum	*vs.* NHE
$ZrTiCO_2$-I	4.24	-1.77	1.29	-4.73	0.23	-0.08	-6.09	1.59
$ZrHfCO_2$-I	3.99	-1.61	1.59	-4.01	-0.49	-0.12	-5.72	1.22
$ZrHfCO_2$-III	4.21	-2.47	1.52	-5.16	0.66	-0.25	-6.93	2.43
$HfTiCO_2$-I	3.69	-2.19	1.24	-4.65	0.15	-0.19	-6.08	1.58
$HfTiCO_2$-III	3.92	-3.35	1.83	-5.43	0.93	-0.10	-7.37	2.87

Table S4 Effective mass $|m^*|$, deformation potential constant $|E_l|$, in-plane stiffness C, and carrier-mobility μ for electrons and holes along the x and y directions.

		C (N/m)	$\|E_l\|$ (eV)	$\|m^*\|$ (m_e)	μ($cm^2 \cdot V^{-1} \cdot s^{-1}$)
$ZrTiCO_2$-I	Electron (x)	280	0.08	16.45	2296
	Hole (x)	280	2.68	0.16	21621
	Electron (y)	253	4.56	4.21	10
	Hole (y)	253	2.38	1.08	544
$ZrHfCO_2$-I	Electron (x)	289	7	1.92	23
	Hole (x)	289	3.84	0.18	8589
	Electron (y)	258	3.08	2.31	72
	Hole (y)	258	1.18	1.15	1989
$ZrHfCO_2$-III	Electron (x)	267	11.34	2.76	4
	Hole (x)	267	9.82	0.30	437
	Electron (y)	240	2.42	2.65	83
	Hole (y)	240	0.52	2.16	2701
$HfTiCO_2$-I	Electron (x)	267	3.58	2.99	33
	Hole (x)	267	0.58	13.23	64
	Electron (y)	240	8.04	3.93	3
	Hole (y)	240	10.22	1.16	24
$HfTiCO_2$-III	Electron (x)	262	4.02	2.81	29
	Hole (x)	262	6.3	0.69	197
	Electron (y)	234	0.16	2.57	19649
	Hole (y)	234	1.88	1.46	441